



Asteroid impact effects on Snowball Earth

Christian KOEBERL ^{1,2*} and Boris A. IVANOV ³

¹Department of Lithospheric Research, University of Vienna, Althanstrasse 14, A-1090 Vienna, Austria

²Natural History Museum, Burgring 7, A-1010 Vienna, Austria

³Institute for Dynamics of Geospheres, Russian Academy of Sciences, 119334 Moscow, Russia

*Corresponding author: E-mail: christian.koerberl@univie.ac.at

(Received 05 August 2018; revision accepted 23 March 2019)

Abstract—Several Snowball Earth periods, in which the Earth has been (almost) totally glaciated, are known from Earth history. Neither the trigger for the initiation, nor the reason for the ending of such phases, are well understood. Here we discuss some mechanical effects of the impact of asteroids 5–10 km in diameter on the Snowball Earth environment. An impact of this scale is the largest impact that is statistically predictable for 10–60 Myr time periods. The impact cratering itself (shock waves, impact crater formation) is not powerful enough to change the natural climate evolution path on Earth. However, the products of impact (mainly—water vapor) can be quickly distributed over a substantial part of the globe, influencing the global circulation (e.g., facilitating cloud formation). It is a question for future studies to confirm if such an event (which is possible statistically during this interval) may or may not have influenced the global climate of the Snowball Earth, and/or contributed to deglaciation.

INTRODUCTION

The hypothesis of global glaciations on Earth in the past has been proposed several times during the last century (Mawson 1949; Kirschvink 1992; Eyles and Janaszczak 2004; Williams 2008). Observational evidence supports the idea that the Precambrian Earth's history has episodes of total ice coverage of the planet—see the recent review by Hoffman et al. (2017) and references therein. The modern Snowball Earth hypothesis states that the Sturtian (about 660–710 Ma) and Marinoan glaciations (about 645–655 Ma) were of global extent and lasted, correspondingly, ~60 and ~10 Myr.

Various critical discussions of the Snowball Earth hypothesis and the extent and effects of the glaciations have been made. Most recently, suggestions were made that the effects of Snowball Earth erased a significant part of the earlier geological history, including impact craters, on Earth (Keller et al. 2019). Today the discussion of mechanisms of the onset and cessation of the Snowball period includes many different possibilities, such as volcanic processes (MacDonald and Wordsworth 2017), volcano-magmatic consequences of a single plate to modern plate tectonics transition

(Stern and Miller 2018), changes in the cloud formation efficiency (Abbot et al. 2012; Abbot 2014; Feulner et al. 2015; Lewis et al. 2006, 2007), or flood basalt weathering (Cox et al. 2016).

Kring (2003) proposed to add hypervelocity asteroid impact to the list of possible triggers of the rapid deglaciation. The data of Bodiselitsch et al. (2005), originally intended to constrain the duration of the Marinoan glaciation, can also be interpreted to indicate the presence of a possible impact-related meteoritic component. However, we note that so far no direct geological or geochemical evidence of a large-scale impact near the Snowball period has yet been found (Gyollai et al. 2014, 2017; Peucker-Ehrenbrink et al. 2016).

Most published impact-related climate change models are devoted to the Chicxulub impact structure formation, where emanation of CO₂ and sulfuric gases from vaporized carbonates and evaporates and, less possibly, ejected dust, are believed to play the main role in the climate change at the K–Pg boundary 66 Ma ago (e.g., Pollack et al. 1983; O'Keefe and Ahrens 1989; Pope et al. 1994, 1997; Pierazzo et al. 2003).

The only known late Neoproterozoic impact structure (<http://www.passc.net/EarthImpactDatabase/>

Agessort.html) is Strangways, Northern Territory, Australia, with a measured age of 646 ± 42 Ma (Spray et al. 1999). From remnants of about 10 km diameter central uplift we can assume an original crater diameter of ~ 40 km, relying on the analogy with the well-studied Puchezh-Katunki impact crater (Ivanov 2007), in parallel with original estimates by Shoemaker and Shoemaker (1996), and in contrast with the 24–26 km diameter mentioned by other authors (Spray et al. 1999; Zumsprekel and Bischoff 2005; Glikson 2018). We do not know if such an impact could have affected the Snowball thermo-atmospheric dynamics. To test the problem, we provide here some impact ideas presented earlier only as abstracts at several meetings (Koeberl et al. 2007a, 2007b). However, we are still unable to test the whole impact trigger scenario. Having some intermediate results, which we want to share with the community, we estimate (1) the probability of an impact of the proper scale occurring during the required time period and (2) the numerical modeling of general consequences of the impact (cratering, oceanic splash, water vapor ejection). We hope these results could be useful for the future GSM modeling (or similar climate change estimates). We are aware that the impact triggering of the Snowball “melting” does not look very attractive today, and may be rejected in the future, but should at least be discussed.

CRATERING RATE ON EARTH AND THE SNOWBALL PERIOD DURATION

The cratering rate on Earth and its possible variation in time has been analyzed before and presented in numerous papers (Neukum et al. 2001; Werner and Ivanov 2015; Bottke et al. 2018). Here we use the most straightforward estimates resulting from the translation of the well-established lunar cratering chronology to Earth, taking into account the relative probability of impacts on both planetary bodies (Ivanov 2006, 2007; Ivanov and Hartmann 2007). These estimates are verified with the dating of many recognized terrestrial impact craters. Previously, the approximate estimates of impact frequency related to Snowball periods has been published by Kring (2003).

Figure 1 presents the cumulative global number $N_{\text{cum}}(> D)$ of the terrestrial craters larger than the given diameter D would be accumulated globally (impacts into ocean are presented with an equivalent crater diameter on land). The balance of a size-dependent erosion of older craters and the new crater formation limits the number of old impact craters that can be found on continents. The plate tectonic lithosphere motion and the oceanic crust subduction erase cratering records for large oceanic impacts. Small impacts do not penetrate the deep ocean water and do not form a crater on the sea floor.

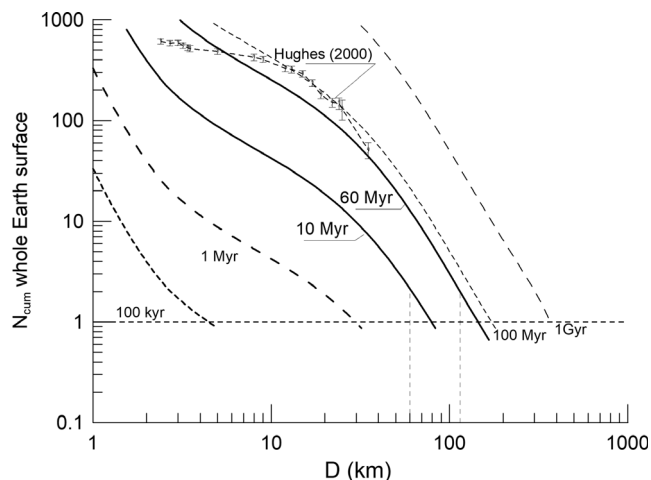


Fig. 1. Cumulative global production number of impacts, measured in equivalent crater diameter on land, for various time intervals. The estimated accuracy is about a factor of 2. Statistically, during the characteristic time period of 10 Myr a few (2 ± 1) impacts may occur with the energy suitable to create a ~ 60 km crater on land, while for 60 Myr a possible land impact crater has diameter about 120 km (vertical dashed lines at D axis). Black triangles are for dated terrestrial craters at surfaces not older than ~ 125 Ma (Hughes 2000). Adapted from Ivanov (2007).

Tentatively the “largest statistically possible” impact during the “Snowball” time periods (or at the very end) for a duration of 10–60 Ma should create a crater on land with a diameter of ~ 60 to ~ 120 km. Hence, we can bracket the trial variant of our estimates with these crater diameters.

The scaling laws of impact cratering allow us to estimate an asteroid’s diameter provided the impact velocity corresponds to typical values of ~ 15 to 20 km s^{-1} . This gives an asteroid diameter range from ~ 4 to 10 km. The direct numerical models of known terrestrial craters, fitted to observations, give, for example, the estimated size of a vertical asteroid projectile of 8 km (at 15 km s^{-1}) for the Popigai impact crater with a diameter of ~ 90 to 100 km (Ivanov 2007). The corresponding energy delivered with this impact is about $8 \times 10^{22} \text{ J}$. Terrestrial impact craters with diameters from 60 to 120 km assume delivery of $\sim 10^{22}$ to 10^{23} J to Earth. At an impact velocity of 16 – 20 km s^{-1} , this energy range corresponds to projectile sizes in the range of 5 – 10 km ; we use an impact velocity of 18 km s^{-1} , for the reconnaissance numerical modeling of impacts.

The kinetic energy range, estimated above, may be compared with solar radiative energy that reaches a disk the size of Earth’s radius. For the solar constant of 1300 W m^{-2} , the time to obtain 10^{22} to 10^{23} J is about 1 – 10 days. Even taking into account the planet’s

albedo, the assumed impact energy seems to be too low to affect the atmospheric circulation directly. Effects with possible feedback could be candidates for the Snowball/impact coupling.

IMPACT ACTION AND ITS MODELING

The general scenario of high-velocity impact effects on the terrestrial environment is described by Toon et al. (1997). Listing various mechanisms of environmental consequences of large-scale effects, Toon et al. (1997) briefly discussed the production of climatically important gases and dust. In the case of oceanic impact, the most obvious effect is due to voluminous water vapor injection above the atmospheric scale height (Birks et al. 2007). It is relatively easy to estimate the amount of vaporized water, but less obvious is the initial distribution of the water vapor plume across the globe.

Water Vapor Production

General estimates of the amount of water, vaporized due to a high-velocity impact as a function of the initial kinetic energy of a projectile, were published by Toon et al. (1997) and started from a formalism proposed by Zahnle (1990). Kring (2003) estimated the water vapor injection on the order of 10^4 Gigatons (10^{16} kg) for an impact event that is statistically possible during the Snowball period. Below we compare these estimates with a few published results of the hydrocode impact modeling and with our own numerical modeling conducted for more detailed insight into the process of the water vapor injection to the atmosphere.

Ahrens and O'Keefe (1983) and Ahrens and O'Keefe (1987) modeled the impact of asteroids and comets into a 5 km deep ocean for an impact event comparable with the Chicxulub cratering event. They also presented data about vapor mass that reached various maximum altitudes. Altitudes are estimated here from ballistic motion of material leaving the computational grid. Shuvalov and Trubetskaya (2007) modeled oceanic impacts for the case when the ocean floor does not influence water impact vaporization (such as at the Eltanin impact event). Pierazzo et al. (1998) simulated the Chicxulub crater formation, devoting special attention to the amount of various gases (including water vapor) released into the atmosphere. Here the source of target water is a combination of shallow surface water (on the order of 100 m deep) and ~20% (by mass) of water from porous sediments.

We used the hydrocode SALEB as available to us to visualize the impact event and to make preliminary

estimates of some qualitative parameters. This hydrocode has a limited ability to compute multi-material problems: currently SALEB can handle three materials #1 and #2, or materials #2 and #3. This fact forces us to compute several models to study the displacement of rock basement, water/ice, and terrestrial atmosphere in a set of trial runs. Technical details of the numerical modeling are published elsewhere (Ivanov et al. 2010; Ivanov and Pierazzo 2011).

We have conducted several model runs to touch the problem of water vapor ejection after a high-velocity impact. The first model problem tackles the relatively high-resolution modeling of the layered target vaporization and vapor ejection to space. The second model problem treats the first minutes of the vapor plume collapse over the atmosphere.

First Model Problem

Set #1 includes the modeling of a rocky asteroid impact into a layered target: H₂O layer (ocean) over a crystalline basement. Equations of state are ANEOS-computed tables for multiphase H₂O (water, water vapors, and seven ice phases), granite, and dunite (Benz et al. 1989; Pierazzo et al. 1997; Ivanov 2005). In this set the atmosphere is not present, so the model set #1 allows us to estimate the maximum amount of H₂O ejected (and ballistically transported) above a given altitude.

The typical initial geometry of the model is presented in Figs. 2 and 3.

Typically, the numerical model has a problem computing large space volumes with a high resolution. In the presented modeling set, we have controlled the resolution problem computing the very early stage of impact with the resolution of 50 CPPR (cells per projectile radius), decreasing the resolution to trace later stage effects. Figure 4 compares the same time moment for different problem resolution.

As can be seen in Fig. 4, the general character of the motion is the same at all resolutions; however, the lower resolution produces a bit less vapor, and does not resolve most hot volumes of the uprising plume. However, even the lowest resolution of 13 CPPR allows us to trace the water plume with a volume accuracy of less than a factor of 2.

To express the amount of water in the plume, we plot the volume of water/water vapor and rocks, uplifted above the given altitude over the surface. The vapor quantity is presented as the volume of ejected, V_{ej} , at the initial density, ρ_0 , (~ 1000 kg m⁻³ for H₂O and 2630 kg m⁻³ for granite). Hence, the corresponding mass is evaluated as $M_{ej} = \rho_0 V_{ej}$.

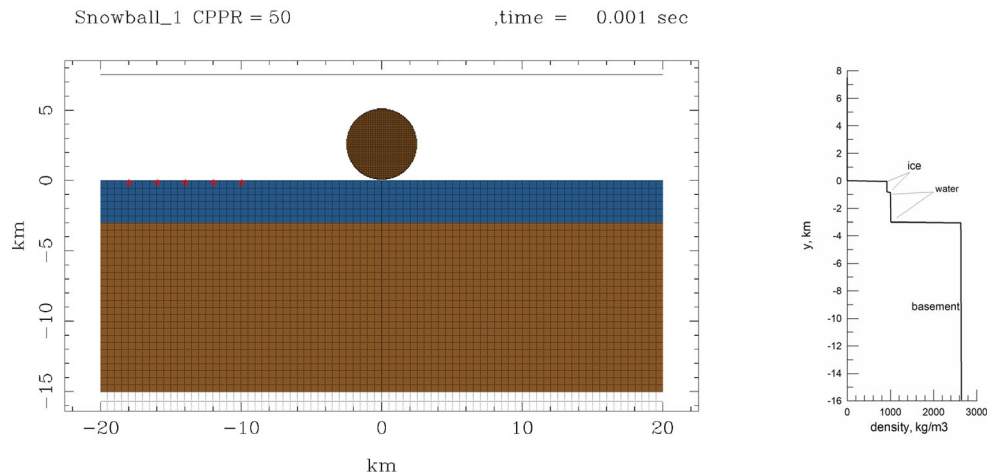


Fig. 2. The geometry for the set #1a: 3 km ocean over crystalline basement. The right panel presents the vertical density profile through the target. The upper 800 m of ocean are frozen to ice — I h ($t = -10^{\circ}\text{C}$, the rest of the target has $t = +10^{\circ}\text{C}$). The resolution is 50 cells per projectile radius. The impact velocity is 18 km s^{-1} . (Color figure can be viewed at wileyonlinelibrary.com.)

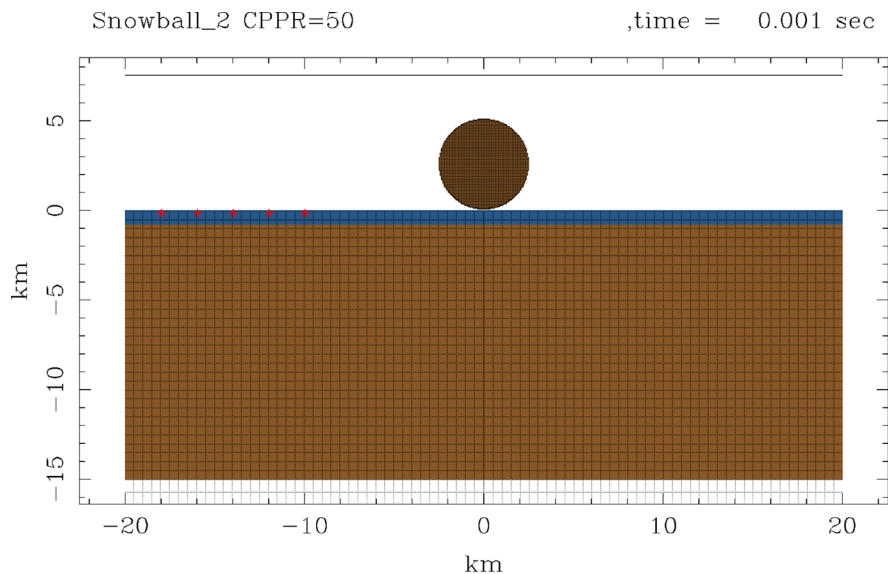


Fig. 3. The geometry for the #1b modeling set: target is present as an ice layer of 800 m over the crystalline basement. The impact velocity is 18 km s^{-1} . (Color figure can be viewed at wileyonlinelibrary.com.)

Figure 5 shows the outcome for the model problem set #1a. The altitude of 50 km is the upper boundary of the computational grid. It is the open boundary and all the material that crossed the boundary is eliminated from the following modeling. The water vapor plume above 10 km altitude reaches its maximum mass ~ 1 min after the impact and 10 s later for 20 km altitude. Here the projectile volume is 75 km^3 and the maximum H_2O mass above 20 km altitude is estimated as $30(V_{\text{ej}}/V_{\text{proj}}) \times 75 (\text{km}^3) \times 10^9 (\text{m}^3 \text{ km}^{-3}) \times 10^3 (\text{kg m}^{-3}) = 2.25 \times 10^{15} \text{ kg}$. The mass leaving the computational grid (to the

assumed upper atmosphere) is smaller by a factor of about 2.

The problem set #1b (800 m ice sheet over the crystalline basement) produces less ejected water vapor due to a smaller volume of initially compressed ice (Fig. 6).

The projectile diameter increase from 5 to 10 km does not result in a proportional increase of the water plume production, as the thickness of ice/water layer is assumed to be the same. To illustrate this fact, the H_2O ejection curves are compared in Fig. 7 for the same

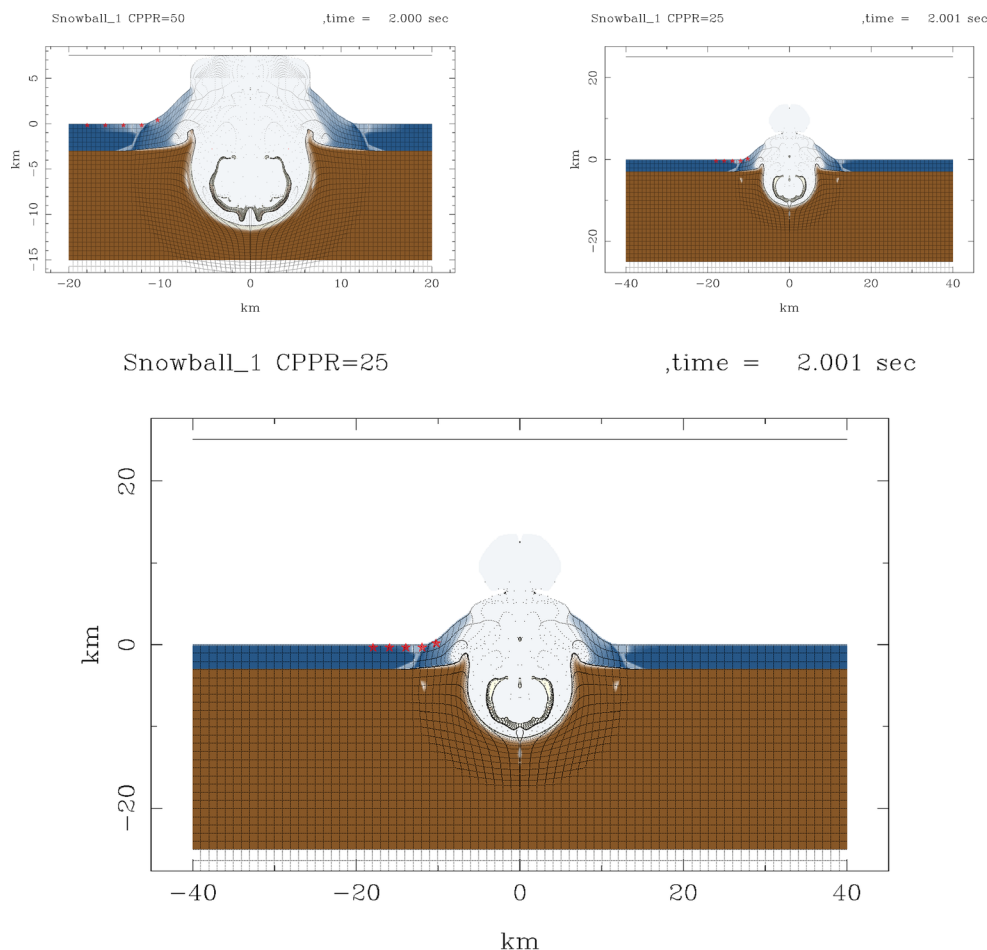


Fig. 4. The comparison of the model set #1a at $t = 2$ s after impact modeled with a resolution of 50 CPPR and $\Delta x = 50$ m (upper left panel), 25 CPPR and $\Delta x = 100$ m (upper left panel), and 13 CPPR and $\Delta x = 200$ m. $D_{\text{proj}} = 5$ km, $v_{\text{imp}} = 18 \text{ km s}^{-1}$. (Color figure can be viewed at wileyonlinelibrary.com.)

target geometry (Fig. 8). The left vertical axis is for the 5 km projectile case, while the right axis is for a 10 km projectile case. Relative units on the left and right vertical axes are chosen so that the maximum relative volumes are the same in both cases. The relative ejected volume decreases roughly by a factor of 2 in the 10 km projectile case. However, the projectile volume itself increases by a factor of 8 ($=2^3$). Hence, the absolute mass of ejected H_2O increases by a factor of 4 (roughly proportional to the projectile cross-sectional area) for double the projectile diameter.

The absolute maximum mass of H_2O , ejected above 20 km in the 10 km projectile case, is about $15(V_{\text{ej}}/V_{\text{proj}}) \times 591(\text{km}^3) \times 10^9(\text{m}^3 \text{ km}^{-3}) \times 10^3(\text{kg m}^{-3}) = 8.9 \times 10^{15} \text{ kg}$.

Second Model Problem

The second model problem is computed to visualize the water vapor plume rise and collapse over the

atmosphere during the first minutes after impact. As the hydrocode in use is capable to treat only two different materials in one computational cell, we simplify the geometry by replacing the rock basement with the rigid lower boundary of the computational grid. The material #1 here is the H_2O in all possible forms (ice, water, vapor), while the material #2 is atmospheric dry air modeled with the ANEOS code (library input).

To balance the spatial resolution and the size of a computational grid, we use the cell size 0.5×0.5 km in the central part of the computational grid, gradually expanding the cell size to 5×5 km at the grid periphery.

The ice projectile with a diameter of 14.6 km impacts vertically in to the ice target at 18 km s^{-1} . The kinetic energy delivered to the target is close to the kinetic energy of 10 km in diameter asteroid with the same impact velocity. Figure 8 shows the central part of the grid 11 and 43 s after the impact.

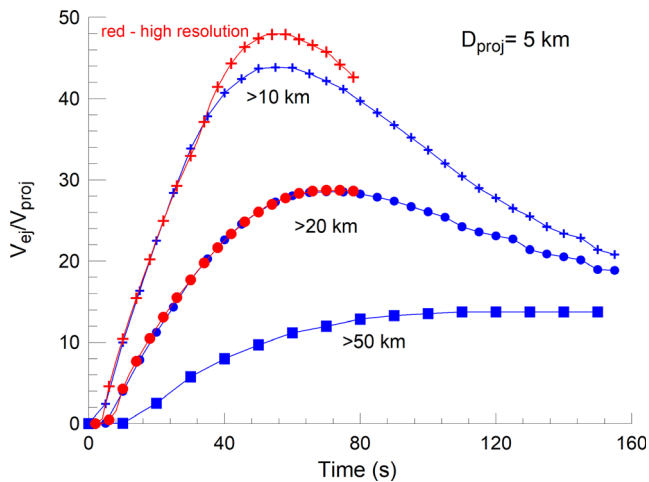


Fig. 5. The ejected volume of H₂O in the model set #1a (3 km ocean, no atmosphere, ejecta decelerates by gravity field only). Red dots are for resolution model run with twice the resolution as for the blue dots. (Color figure can be viewed at wileyonlinelibrary.com.)

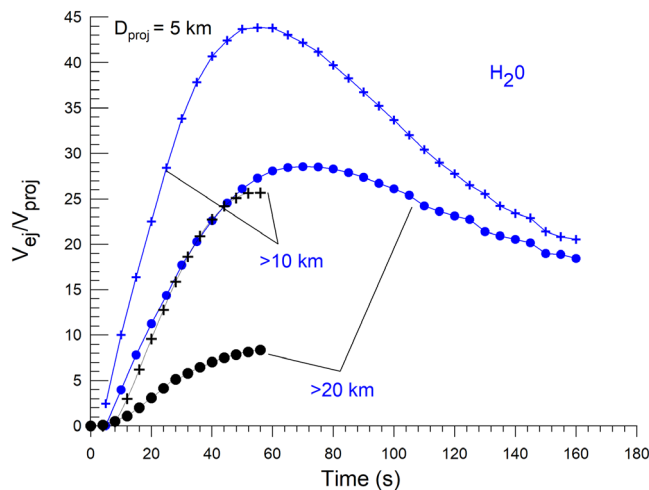


Fig. 6. The comparison of H₂O ejection in model problem sets #1a (blue) and #1b (black). The presence of 800 m ice layer results in roughly half the amount of H₂O ejected ballistically above a given altitude. (Color figure can be viewed at wileyonlinelibrary.com.)

The upper boundary of the grid is a free-outflow boundary: the material can leave the grid, but cannot return back. The control of outflow through the upper boundary gives a maximum of 10% of the vapor plume to leave the grid.

Figure 9 illustrates the late time of the modeling. Figure 10 compares analytical estimates from Toon et al. (1997) with the results of the aforementioned selected publications. In general, we see a very good

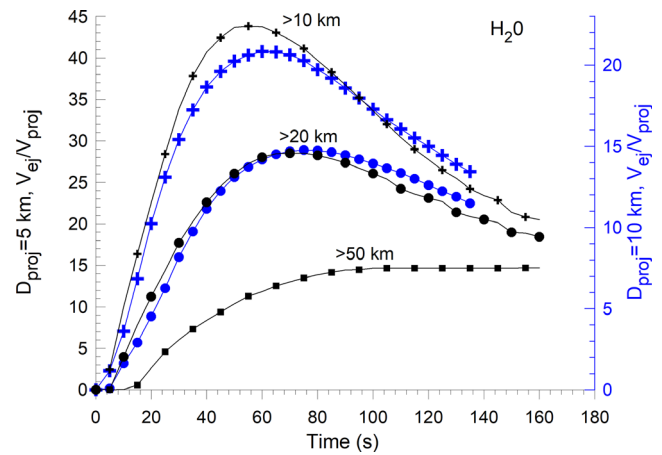


Fig. 7. Comparison of 5 and 10 km projectile impacts. See text for details. (Color figure can be viewed at wileyonlinelibrary.com.)

coincidence with the analytical relations derived by Toon et al. (1997). However, only Ahrens and O'Keefe (1983, 1987) published estimates of the altitudes that were reached by various fractions of the water vapor plume. For this reason, we conducted a few model runs as a start for more detailed analyses that might be performed in the future.

Our results for water vapor amount in the plume are close to previously published data (Fig. 10). Figure 10 shows only estimates of H₂O mass delivered to altitudes >10 km. This value is chosen as a proxy to the estimated equatorial Snowball tropopause 6–8 km altitude (Abbot et al. 2013; Hoffman et al. 2017).

The main impression from our relatively simple modeling is that a high-velocity asteroid impact delivers 10^{15} – 10^{16} kg of water vapor to high altitudes (>20 km). Two trivial visible trends are as follows. (1) Large mass of ejected water vapor in oceanic impacts (versus an impact into the relatively thin ice-covered continent) and (2) an increase of ejected water vapors with the assumed asteroid size.

In contrast to Ahrens and O'Keefe (1983), we have tried to make a direct insight into the style of water vapor plume collapse over the ambient atmosphere. Taking into account the usual conflict of resolution versus spatial coverage (small cell size and wide grid boundaries), we have computed the impact of a relatively large ice projectile over the icy hemisphere covered by the terrestrial atmosphere. Selected qualitative results are discussed below.

DISCUSSION

Most of published impact-related climate change models are devoted to the Chicxulub impact crater

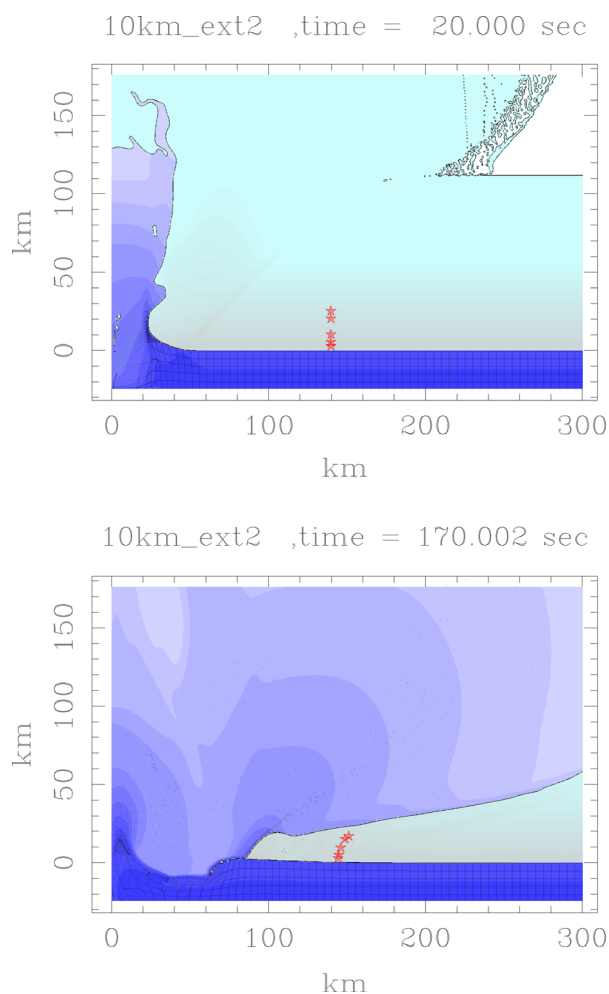


Fig. 8. The water plume geometry at 20 s (upper frame) and 170 s (lower frame) after the impact. The blue color intensity logarithmically reflects rarefaction of expanding vapors. Atmosphere (bluish gray) is trapped under falling and expanding vapors. Red stars show Lagrangian tracers with detailed thermodynamic history recording. The initial atmosphere is set with the upper boundary of ~ 100 km above the surface. The shock waves and the expanding plume accelerate a huge bubble of rarified air to a high velocity. This ejected air travels ahead of the expanding plume. (Color figure can be viewed at wileyonlinelibrary.com.)

formation, where emanation of CO_2 and sulfuric gases from vaporized carbonates and evaporates and, less possibly, ejected dust, are believed to play the main role in the climate change at the K–Pg boundary 66 Ma ago (Pollack et al. 1983; O’Keefe and Ahrens 1989; Pope et al. 1994, 1997; Pierazzo et al. 2003).

Water Vapor Plume

Melosh (1990) discussed the role of impact-generated vapor plumes in the whole list of impact-related phenomena as a “neglected aspect of impact

cratering.” Within a few years, intensive investigations on impact-generated gaseous plumes have been started to analyze observational data for impacts of the Shoemaker-Levy IX cometary fragments to Jupiter (Carlson et al. 1997). Numerical modeling revealed the formation of hundreds-km gaseous plumes ejected above 1 bar level (“surface”) rises up and collapsed in a time scale of 10 min. Similar events were predicted and analyzed for impacts into the terrestrial atmosphere (Boslough and Crawford 1997; Shuvalov 1999; Artemieva and Shuvalov 2007). Previous studies on impact plumes on Jupiter and Earth mostly considered the heated atmospheric gas. Even in this case, the fallback of the ejected plume may cause high-altitude atmospheric heating and oscillations (Nemtchinov and Loseva 1994).

For large crater-forming events on Earth when large amounts of solid material can be ejected, the re-entry of dense fragments has been treated theoretically (Melosh et al. 1990; Goldin and Melosh 2007, 2008). In the case of impact into a continental ice glacier or in the ocean (covered or not covered by ice), the important role is played by ejected water vapor in the excitation of the terrestrial atmosphere. The vapor plume rises well above the limit of the atmosphere, expands laterally, and collapses in the gravity field over the ambient atmosphere. The interaction of the collapsing plume with the atmosphere resembles the entry of a dust plume (Goldin and Melosh 2007, 2008): at some altitude above the surface, the air density is large enough to decelerate the collapsing plume. Plume material decelerates and compresses the air. The air compression results in heating of the atmosphere. The excess thermal energy is partially removed by a radiation transfer (mainly in infrared), and partially is redistributed by turbulent mixing. If the plume material density is larger than the atmospheric air density at the boundary between plume and atmosphere, the gravity instability initiates density currents—downward streams of heavier material (Goldin and Melosh 2007, 2008).

All these processes are not easy to model. In our simplified modeling of the water vapor plume collapse, intimate details of the plume/atmosphere mixing are not resolved properly due to (1) low spatial resolution (cells 0.5×0.5 km) and (2) due to lack of kinetics in the description of vapor crystallization during almost ballistic flight above atmosphere. Nevertheless, we believe that even the semiquantitative results of our preliminary modeling may be useful for any further clarification of this complex process.

According to preliminary model runs with a relatively wide computational grid (500 km in height and ~ 2000 km in radial direction), the water plume is accelerated by initially high thermal pressure, expands

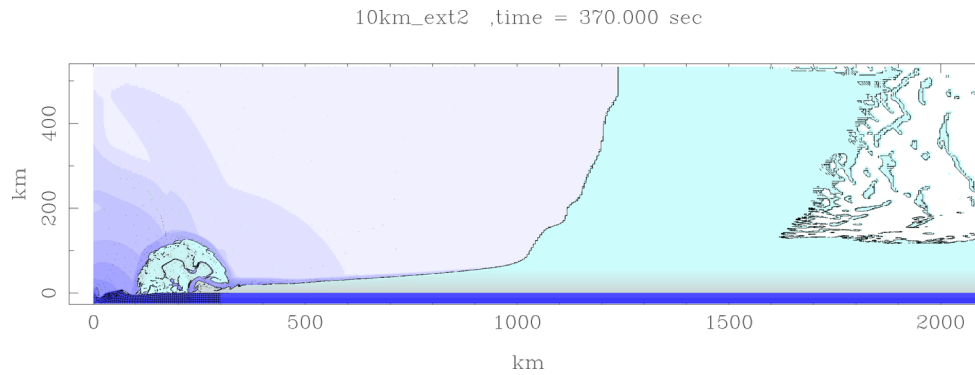


Fig. 9. Approximately 6 min after the impact, the collapsing vapor plume expands ~ 1000 km from the impact point. The final mass redistribution needs much more time, including the fall of “off-grid” most fast part of the plume. These parts of the (condensed) water vapor ejected to high altitudes according to ballistic estimates fall back to the atmosphere within 30 min and cover an area of ~ 2000 km in radius (4000 km in diameter). The atmosphere trapped under the water cloud at distances of 200 ± 100 km is “blowing up”—although this most probably is a computational artifact, caused by incomplete treatment of small volume concentrations in mixed cells. The space above the atmosphere (initial upper atmosphere boundary at ~ 100 km) and beyond the water plume is filled with highly rarefied air ejected at early times (see upper panel in Fig. 8). (Color figure can be viewed at wileyonlinelibrary.com.)

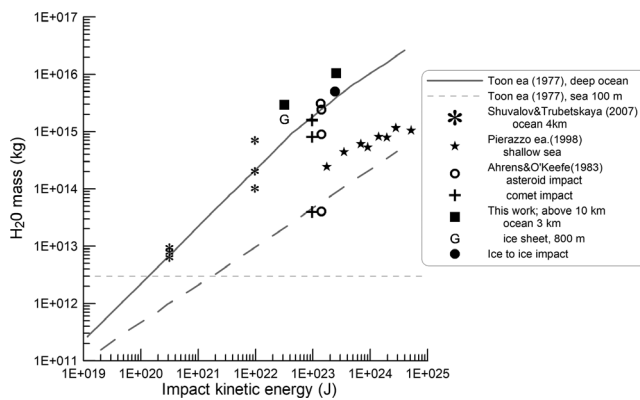


Fig. 10. Review of impact water vaporization and ejection to the upper atmosphere from individual numerical modeling in this work and by Ahrens and O’Keefe (1983, 1987), Pierazzo et al. (1998), and Shuvalov and Trubetskaya (2007) in comparison with the analytical model of Toon et al. (1997), shown as a solid curve for impacts into a deep ocean and as a dashed curve for impacts into a shallow (100 m) sea. The horizontal dashed line is the approximate global water content in the modern terrestrial atmosphere. A set of the same signs for individual models shows the estimated range of water mass delivered at altitudes higher than 10, 50, and 100 km (top to bottom, respectively).

fast above the atmosphere, cools down due to isoentropic decompression, and flights out in the terrestrial gravity field. After expansion, the vapor temperature drops down below the boiling/sublimation value and the plume vapors are moving in a partially condensed (saturated) state. Part of the atmosphere, pushed out by the plume breakthrough, moves ahead of the expanding plume (but we are not sure whether the

flow of extremely rarefied gas is well modeled with the hydrocode in use). At radial distances of a few hundred km and further, the effective vertical downward velocity near to the boundary of the atmosphere is a few km s^{-1} (Fig. 11). The deceleration of collapsing plume material occurs at altitudes of 20–50 km, and the atmosphere below is heated.

The model run is stopped at the time moment of 390 s (6.5 min) after impact. At this moment, the water vapor cloud is expanded to ~ 1100 km radially, and mostly collapsed over the atmosphere. The vapor mass per unit area exponentially decreases with distance (Fig. 12). Only in close vicinity to the impact site (< 400 km), the collapsed vapor mass is comparable with the atmospheric column mass. However, at radial distances up to ~ 1000 km, the plume mass is a few orders of magnitude above the level of the modern water vapor mass in the upper atmosphere (Toon et al. 1997).

The presented model run covers only the first ~ 390 s after the impact, and some further redistribution of water vapor occurs later. However, the hydrocode in use cannot reliably cover these later times due to restrictions in spatial resolution and improper description of highly rarefied gas motion in the gravity field. The total amount of water in the computational grid begins to decrease when the expanding vapor plume reaches the upper “free outflow” computational grid boundary. The total H_2O mass ejected beyond this boundary placed near altitude of 500 km is about 0.4×10^{15} kg, which is approximately 10% of $\sim 4 \times 10^{15}$ kg of water/vapors inside the computational grid beyond radial distance of 100 km. The recorded

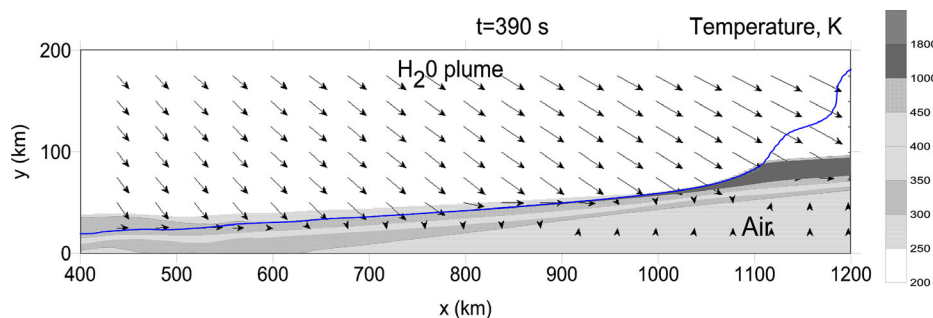


Fig. 11. Periphery (radial distances >400 km) of the collapsing plume. The velocity vector scale is chosen so that 1 km s^{-1} corresponds to 10 km of the linear scale. Nonlinear temperature scale is shown to the right. Within ~ 650 km radial distance, the atmosphere is compressed into a $20\text{--}30$ km layer and heated to temperatures above ~ 300 to 350 K (~ 30 to 80°C). The upper atmosphere at the lower plume boundary may be heated to $\sim 1000 \text{ K}$. (Color figure can be viewed at wileyonlinelibrary.com.)

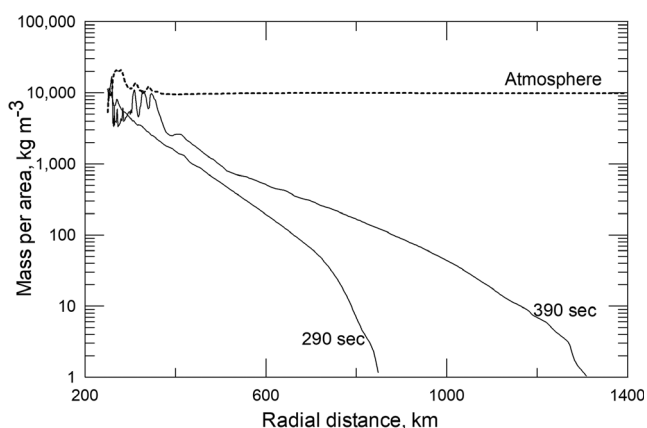


Fig. 12. Water vapor (black curves) and air (dashed curve) column mass (mass per unit area) versus radial distance in two moments of time separated at 100 s . Ambient upper atmosphere water (for the modern atmosphere) is about $10^{-2} \text{ kg m}^{-2}$ (Toon et al. 1997), two orders of magnitude below the horizontal axis.

outflow through the upper grid boundary and the particle velocity at the moment of the boundary crossing allow us estimate distances of the ballistic flight, not computed directly in the model. Results show that the maximum outflow rate ($\sim 2.6 \times 10^{11} \text{ kg s}^{-1}$) is reached $\sim 150 \text{ s}$ after the impact, with a mass-weighted average velocity of 4 km s^{-1} inclined at the mass-averaged angle of 60° above horizon. The maximum radial deposition distance of this “extra-grid” water cloud is about 2500 km ($\sim 20^\circ$ of angular distance along the globe surface). Fifty percent of this “extra-grid” mass is deposited in an annular ring between 600 and 1200 km from the impact site. The material returns to the Earth’s surface (to the lower atmosphere) at times 500 to 1000 s after the impact—much later than the duration of the presented model run (390 s).

The average column mass of the total amount of water vapors deposited within radial distance of

2000 km is about 260 kg m^{-2} , which is a factor of 40 less than the atmospheric column mass of $\sim 10,000 \text{ kg m}^{-2}$ (Fig. 12).

Vapor Plume “Contamination”

In the previous subsection, we discussed the main features of the water vapor plume formation, expansion, and deposition. As it was discussed earlier, most of this water returns to the surface relatively quickly (Toon et al. 1997; Kring 2003). However, part of the redistributed water may create a high-altitude enrichment atmosphere with water vapor. Under the action of solar energy, the longer living fraction of the water molecules may dissociate in photochemical reactions. Additional important factors may arise from some “contamination” (or loading) of the water plume with another target species.

The most obvious “contamination” is mineral dust, which is inevitably incorporated in the expanding vapor plume in the case of a continental impact. The dust cloud action has been discussed in detail in numerous publications. The current paradigm is in favor of relatively fast redeposition of dust, a restricted time period of the atmospheric transparency decrease due to dust loading, and the consequent global cooling (Toon et al. 1997; Luder et al. 2003). The fast deposition of sub-mm (and larger) particles is typically discussed as the main reason for a limited influence of the dust impact on the climate (Birks et al. 2007). A supplementary factor to the well-discussed problem of a dust cloud is a possible physico-chemical modification of the rock-forming minerals in the dust/supercritical water mixture cloud. Experiments show that in rock–water mixtures, shock compression leads to the formation of ultrafine (down to 300 nm) particles (Furukawa et al. 2007; Umeda et al. 2017). It is now impossible to make quantitative estimates for a possible

amount of these ultrafines in a real impact cratering event. Here we note only that an impact into an ice-covered continental site produces favorable conditions for the formation of a rock–steam mixture in close vicinity of the impact location.

A less frequently discussed case is the oceanic impact, when the water vapor plume is naturally loaded with salt particles produced from sea salt after the water vaporization (Klumov 2001). In an application to the Snowball Earth, we should take into account that the liquid oceanic water and sea ice with brine/crystalline salty pockets (Carns et al. 2015; Hoffman et al. 2017) could be covered with a fresh meteoric ice (Hoffman et al. 2017). So, vaporization of sea water in an impact is possible only if the vaporization zone penetrates below the non-salted meteoric ice.

The salt particle formation from the salty sea water/ice is strongly accelerated for supercritical water by the process of gradual decompression, when the fluid density and solubility decrease. Under these conditions, the “shock crystallization” has been observed to result in salt particle formation of a few μm in size (Armellini et al. 1994). In other experiments, sub- μm particle formation has been observed (Petersen et al. 1986). The process is now under discussion in a connection with salt formation deep under the ocean (Hovland et al. 2006). In the shock vaporization of water, the compression at the shock front is following with the adiabatic release. For sufficiently high shock pressure, the water thermodynamic state passes above the critical point, and conditions for the fast nucleation of salt particles are achieved. Hence, we can speculate that the sea water in the vapor plume would contain aerosols of condensed salt particles of various chemical compositions. These particles may undergo photochemical reactions due to sunlight irradiation while they float in the upper part of the collapsed plume.

For the nominal sea water salinity of 3.5%, the water vapor plume initially (the first hour after the impact) deposits ~ 2 mass% of Cl, ~ 1 mass% of Na, ~ 0.13 mass% of Mg, and about ~ 0.1 mass% of S. The exact complex chemistry evolution of salt molecules depends strongly on the local pressure and temperature and is not discussed here. We can only note here that for the most powerful water vapor plume modeled in our work, the total water vapor mass redistributed within a circle of about 4000 km in diameter at the globe is about 3×10^{15} kg of H_2O . If all this mass is produced from the nominal ocean water (with the present-day salinity), the vapor plume delivers to the upper atmosphere the following species

- $\sim 6 \times 10^{13}$ kg (=60 Gt) of chlorine,
- $\sim 3 \times 10^{13}$ kg (=30 Gt) of sodium,
- $\sim 4 \times 10^{12}$ kg (=4 Gt) of magnesium,
- $\sim 3 \times 10^{12}$ kg (=3 Gt) of sulfur, and

$\sim 2 \times 10^{11}$ kg (=0.2 Gt) of bromine.

The sulfur mass can be compared with the range from highest (300 Gt) to lowest (30 Gt) of sulfur estimated for the Chicxulub impact event versus recent powerful volcanic eruptions (0.01 to 0.1 Gt of S) (Pinto et al. 1989; Hoff 1992; Pierazzo et al. 2003).

SPECULATIONS AND PRELIMINARY CONCLUSIONS

While most of the scenarios for climate forcing by volcanic eruptions result in global cooling (Ramaswamy 1992; Bendtsen and Bjerrum 2002), the presence of species similar to volcanic ones but delivered above the atmosphere with the heavy water vapor cloud may act differently. We know only the publication by Birks et al. (2007), discussing the consequences of water plume deposition for the upper atmosphere (above an altitude of 30 km), but for impact events that are well below the energy discussed above (ejection of 1.3×10^{39} molecules of water, $\sim 4 \times 10^{13}$ kg, versus $n \times 10^{15}$ kg in the largest impact possible for an assumed Snowball period duration).

The high-velocity impact modeling reveals first estimates of processes and the amount of vaporized water delivered to the atmosphere and above. In the “modest” case of 5 km in diameter asteroid impact into an ocean of 3 km depth, the mass of water vapor delivered above 20 km in the local maximum reaches the value of 2×10^{15} kg. A projectile of twice that size, with 10 km diameter, increases this estimate about four times.

The impact into 800 m thick ice above granitic basement produces a factor of 4 less water vapor in the plume (for the 5 km diameter asteroid). The following fate of the water vapor in the plume depends on the interaction with the atmosphere. We can approximately draft the following general scenarios, including information from Toon et al. (1997) and Birks et al. (2007). (1) An impact occurs in the ice-covered ocean or in the glacier-covered continent, (2) the impact vaporization of ice/water creates a steam plume expanding through and above the atmosphere, and (3) the vapor/snow plume collapses over the atmosphere. In the largest of our models (with the widest spatial boundaries 500 km above the target level and 2000 km from the impact point), the direct pushing out and heating of the atmosphere occurs as far as ~ 200 km from the impact location. At larger distances, the plume deposits vapor/snow over the atmosphere, covering areas 2000–3000 km in radius. The resulted continent-sized “warm spot” in the atmosphere, filled initially with water vapors (condensing while cooling), looks like a reasonable scenario for a trial atmospheric circulation modeling. The set of model cases with salt particles or ultrafine rock mineral dust loading

may be used as additional factors for the surveillance of climate forcing factors.

The model of the vapor plume evolution in the upper atmosphere (Birks et al. 2007) illustrates that for an oceanic impact event with the factor of 1000 lower amount of injected water molecules, the enhanced concentration of water molecules at altitudes of 35–50 km continue to be noticeably elevated in terms of globally averaged values. We can only speculate that injection of much larger volumes of water may (or may not) follow with possible nonlinear effects that are more diverse than just the destruction of the ozone layer. If the decay time of a perturbation is long enough, the unknown feedback effect could result in a relatively long-term climate change. MacCracken (2007) noted in his subsection 16.2.4 that “. . . how this effect would play out climatically has not been simulated, although a relatively strong warming influence for a few years may essentially counterbalance at least part of the relatively large cooling influence from injected dust and soot” (p. 283)

More possible implementation of impact-injected water may be evaluated in the future in line with ideas of cloud importance for the general circulation modeling (Abbot et al. 2012; Abbot 2014; Hoffman et al. 2017). Providing that an assumed impact event adds water to the dry Snowball atmosphere, one may suspect a possible shift toward accelerating of the Snowball melting.

In conclusion, we note that in terms of cratering rates, it is statistically plausible that the impact of a 5–10 km diameter asteroid occurred during a “Snowball period.” However, progress has been slow in our understanding of such a hypothetical large-scale impact could initiate or accelerate the Snowball deglaciation, following the first published estimates on this topic (Kring 2003). Definitely, more impact and climatic simulations are needed to confirm or reject possible effects of an impact event on the atmosphere in a Snowball Earth.

Acknowledgments—The second author (B. A. I.) is supported by Program 28, Russian Academy of Science Presidium. We thank J. Goodman for input into earlier versions of this project. Part of this work was conceived when B. A. I. was a visiting professor at the University of Vienna. We dedicate this paper to our friend and colleague Uwe Reimold. We are grateful to H. J. Melosh and P. F. Hoffman for critical and constructive reviews.

Editorial Handling—Dr. Jeffrey Plescia

REFERENCES

- Abbot D. S. 2014. Resolved snowball Earth clouds. *Journal of Climate* 27:4391–4402.
- Abbot D. S., Voigt A., Branson M., Pierrehumbert R. T., Pollard D., Le Hir G., and Koll D. D. B. 2012. Clouds and snowball Earth deglaciation. *Geophysical Research Letters* 39: L20711_1–L20711_4, <https://doi.org/10.1029/2012gl052861>
- Abbot D. S., Voigt A., Li D., Le Hir G., Pierrehumbert R. T., Branson M., Pollard D., and Koll D. D. B. 2013. Robust elements of Snowball Earth atmospheric circulation and oases for life. *Journal of Geophysical Research (Atmospheres)* 118:6017–6027.
- Ahrens T. J. and O’Keefe J. D. 1983. Impact of an asteroid or comet in the ocean and extinction of terrestrial life. *Journal of Geophysical Research* 88:799.
- Ahrens T. J. and O’Keefe J. D. 1987. Impact on the Earth, ocean and atmosphere. *International Journal of Impact Engineering* 5:13–32.
- Armellini F. J., Tester J. W., and Hong G. T. 1994. Precipitation of sodium chloride and sodium sulfate in water from sub- to supercritical conditions: 150 to 550°C, 100 to 300 bar. *The Journal of Supercritical Fluids* 7:147–158.
- Artemieva N. and Shuvalov V. 2007. 3D effects of Tunguska event on the ground and in atmosphere (abstract #1537). 38th Lunar and Planetary Science Conference. CD-ROM.
- Bendtsen J. and Bjerrum C. J. 2002. Vulnerability of climate on Earth to sudden changes in insolation. *Geophysical Research Letters* 29:1-1–1-4.
- Benz W., Cameron A. G. W., and Melosh H. J. 1989. The origin of the Moon and the single-impact hypothesis III. *Icarus* 81:113–131.
- Birks J. W., Crutzen P. J., and Roble R. G. 2007. Frequent ozone depletion resulting from impacts of asteroids and comets. In *Comet/asteroid impacts and human society*, edited by Bobrowsky P. T. and Rickman H. Berlin: Springer. pp. 225–245.
- Bodiselsitch B., Koeberl C., Master S., and Reimold W. U. 2005. Estimating duration and intensity of Neoproterozoic snowball glaciations from Ir anomalies. *Science* 308:239–242.
- Boslough M. and Crawford D. 1997. Shoemaker-Levy 9 and plume-forming collisions on Earth. *Annals of the New York Academy of Sciences* 822:236–282.
- Bottke W. F., Mazrouei S., Ghent R. R., Parker A. H., and Gernon T. M. 2018. What really happened to Earth’s older craters? (abstract #1457). 49th Lunar and Planetary Science Conference. CD-ROM.
- Carlson R. W., Drossart P., Encrenaz T., Weissman P. R., Hui J., and Segura M. 1997. Temperature, size, and energy of the Shoemaker-Levy 9 G-Impact fireball. *Icarus* 128:251–274.
- Carns R. C., Brandt R. E., and Warren S. G. 2015. Salt precipitation in sea ice and its effect on albedo, with application to Snowball Earth. *Journal of Geophysical Research: Oceans* 120:7400–7412.
- Cox G. M., Halverson G. P., Stevenson R. K., Vokaty M., Poirier A., Kunzmann M., Li Z.-X., Denyszyn S. W., Strauss J. V., and MacDonald F. A. 2016. Continental flood basalt weathering as a trigger for Neoproterozoic Snowball Earth. *Earth and Planetary Science Letters* 446:89–99.
- Eyles N. and Januszczak N. 2004. “Zipper-rift”: A tectonic model for Neoproterozoic glaciations during the breakup of Rodinia after 750 Ma. *Earth-Science Reviews* 65:1–73.

- Feulner G., Hallmann C., and Kienert H. 2015. Snowball cooling after algal rise. *Nature Geoscience* 8:659–662.
- Furukawa Y., Nakazawa H., Sekine T., and Kakegawa T. 2007. Formation of ultrafine particles from impact-generated supercritical water. *Earth and Planetary Science Letters* 258:543–549.
- Glikson A. 2018. Structure and origin of Australian ring and dome features with reference to the search for asteroid impact events. *Tectonophysics* 722:175–196.
- Goldin T. J. and Melosh H. J. 2007. Interactions between Chicxulub ejecta and the atmosphere: The deposition of the K/T double layer (abstract #2114). 38th Lunar and Planetary Science Conference. CD-ROM.
- Goldin T. J. and Melosh H. J. 2008. Chicxulub Ejecta Distribution: Patchy or Continuous? (abstract #2469). 39th Lunar and Planetary Science Conference. CD-ROM.
- Gyollai I., Mader D., Polgári M., Popp F., and Koeberl C. 2014. Lack of evidence for impact signatures in Neoproterozoic postglacial deposits from NW-Namibia. *Austrian Journal of Earth Sciences* 107:100–111.
- Gyollai I., Polgári M., Fintor K., Pal-Molnar E., Popp F., and Koeberl C. 2017. Microbial activity records in Marinoan Snowball Earth postglacial transition layers connecting diamictite with cap carbonate (Otavi Group, NW-Namibia). *Austrian Journal of Earth Sciences* 110:4–20.
- Hoff R. M. 1992. Differential SO₂ column measurements of the Mt. Pinatubo volcanic plume. *Geophysical Research Letters* 19:175–178.
- Hoffman P. F., Abbot D. S., Ashkenazy Y., Benn D. I., Brocks J. J., Cohen P. A., Cox G. M., Creveling J. R., Donnadieu Y., Erwin D. H., Fairchild I. J., Ferreira D., Goodman J. C., Halverson G. P., Jansen M. F., Le Hir G., Love G. D., MacDonald F. A., Maloof A. C., Martin C. A., Ramstein G., Rose B. E. J., Rose C. V., Sadler P. M., Tziperman E., Voigt A., and Warren S. G. 2017. Snowball Earth climate dynamics and Cryogenian geology-geobiology. *Science Advances* 3: e1600983.
- Hovland M., Kuznetsova T., Rueslåtten H., Kvamme B., Johnsen H. K., Fladmark G. E., and Hebach A. 2006. Sub-surface precipitation of salts in supercritical seawater. *Basin Research* 18:221–230.
- Hughes D. W. 2000. A new approach to the calculation of the cratering rate of the Earth over the last 125±20 Myr. *Monthly Notices of the Royal Astronomical Society* 317:429–437.
- Ivanov B. A. 2005. Shock melting of permafrost on Mars: Water ice multiphase equation of state for numerical modeling and its testing (abstract #1232). 36th Lunar and Planetary Science Conference. CD-ROM.
- Ivanov B. A. 2006. Earth/Moon impact rate comparison: Searching constraints for lunar secondary/primary cratering proportion. *Icarus* 183:504–507.
- Ivanov B. A. 2007. Geologic effects of large terrestrial impact crater formation. In *Catastrophic events caused by cosmic bodies*, edited by Adushkin V. V. and Nemchinov I. V. Berlin, Germany: Springer. pp. 163–205.
- Ivanov B. A. and Hartmann W. K. 2007. Exogenic dynamics, cratering and surface ages. In *Planets and Moons*, edited by Spohn T. Treatise on Geophysics, vol. 10. Amsterdam: Elsevier. pp. 207–242.
- Ivanov B. A. and Pierazzo E. 2011. Impact cratering in H₂O-bearing targets on Mars: Thermal field under craters as starting conditions for hydrothermal activity. *Meteoritics & Planetary Science* 46:601–619.
- Ivanov B. A., Melosh H. J., and Pierazzo E. 2010. Basin-forming impacts: Reconnaissance modeling. In *GSA Special Paper 465: Large meteorite impacts and planetary evolution IV*, edited by Gibson R. L. and Reimold W. U. Geological Society of America. Boulder, Colorado, USA pp. 29–49.
- Keller C. B., Husson J. M., Mitchell R. N., Bottke W. F., Gernon T. M., Boehnke P., Bell E. A., Swanson-Hysell N. L., and Peters S. E. 2019. Neoproterozoic glacial origin of the great unconformity. *Proceedings of the National Academy of Sciences* 116:1136–1145. <https://doi.org/10.1073/pnas.1804350116>.
- Kirschvink J. L. 1992. Late Proterozoic low-latitude global glaciation: The Snowball Earth. In *The Proterozoic biosphere: A multidisciplinary study*, edited by Schopf J. W. and Klein C. Cambridge, UK: Cambridge University Press. pp. 51–52.
- Klumov B. A. 2001. The creation of ozone holes as a consequence of meteoroids falls into the ocean. *Advances in Space Research* 28:1159–1167.
- Koeberl C., Ivanov B. A., and Goodman J. 2007a. Impact-induced deglaciation of the snowball Earth? *EOS Transactions, American Geophysical Union* 88. Fall Meeting Supplement, Abstract U22A-08.
- Koeberl C., Ivanov B. A., and Goodman J. 2007b. Impact triggering of the snowball Earth deglaciation? In Abstracts, International Meeting on: Bridging the Gap II: Effect of Target Properties on the Impact Cratering Process, pp. 62–63.
- Kring D. A. 2003. Environmental consequences of impact cratering events as a function of ambient conditions on Earth. *Astrobiology* 3:133–152.
- Lewis J. P., Weaver A. J., and Eby M. 2006. Deglaciating the snowball Earth: Sensitivity to surface albedo. *Geophysical Research Letters* 33:23,604.
- Lewis J. P., Weaver A. J., and Eby M. 2007. Snowball versus slushball Earth: Dynamic versus nondynamic sea ice? *Journal of Geophysical Research (Oceans)* 112:11,014. <https://doi.org/10.1029/2006JC004037>.
- Luder T., Benz W., and Stocker T. F. 2003. A model for long-term climatic effects of impacts. *Journal of Geophysical Research (Planets)* 108:5074. <https://doi.org/10.1029/2002JE001894>.
- MacCracken M. C. 2007. The climatic effects of asteroid and comet impacts: Consequences for an increasingly interconnected society. In *Comet/asteroid impacts and human society: An interdisciplinary approach*, edited by Bobrowsky P. and Rickman H. Berlin: Springer-Verlag. pp. 277–289.
- MacDonald F. A. and Wordsworth R. 2017. Initiation of Snowball Earth with volcanic sulfur aerosol emissions. *Geophysical Research Letters* 44:1938–1946.
- Mawson D. 1949. The Elatina glaciation: A third recurrence of glaciation evidenced in the Adelaide system. *Transactions of the Geological Society of South Africa* 73:117–121.
- Melosh H. J. 1990. Vapor plumes: A neglected aspect of impact cratering. *Meteoritics* 25:386.
- Melosh H. J., Schneider N. M., Zahnle K. J., and Latham D. 1990. Ignition of global wildfires at the Cretaceous/Tertiary boundary. *Nature* 343:251–254.

- Nemtchinov I. V. and Loseva T. V. 1994. Atmospheric oscillations initiated by the penetration of a comet or an asteroid into gaseous envelope of a planet (abstract). 25th Lunar and Planetary Science Conference. p. 987.
- Neukum G., Ivanov B. A., and Hartmann W. K. 2001. Cratering records in the inner solar system in relation to the lunar reference system. *Space Science Reviews* 96:55–86.
- O'Keefe J. D. and Ahrens T. J. 1989. Impact production of CO₂ by the Cretaceous/Tertiary extinction bolide and the resultant heating of the Earth. *Nature* 338:247–249.
- Petersen R. C., Matson D. W., and Smith R. D. 1986. Rapid precipitation of low vapor pressure solids from supercritical fluid solutions: The formation of thin films and powders. *Journal of the American Chemical Society* 108:2100–2102.
- Peucker-Ehrenbrink B., Waters C. A., Kurz M. D., and Hoffman P. F. 2016. No evidence of extraterrestrial noble metal and helium anomalies at Marinoan glacial termination. *Earth and Planetary Science Letters* 437:76–88.
- Pierazzo E., Vickery A. M., and Melosh H. J. 1997. A reevaluation of impact melt production. *Icarus* 127:408–423.
- Pierazzo E., Kring D. A., and Melosh H. J. 1998. Hydrocode simulation of the Chicxulub impact event and the production of climatically active gases. *Journal of Geophysical Research* 103:28,607–28,625.
- Pierazzo E., Hahmann A. N., and Sloan L. C. 2003. Chicxulub and climate: Radiative perturbations of impact-produced S-bearing gases. *Astrobiology* 3:99–118.
- Pinto J. P., Toon O. B., and Turco R. P. 1989. Self-limiting physical and chemical effects in volcanic eruption clouds. *Journal of Geophysical Research* 94:11,165–11,174.
- Pollack J. B., Toon O. B., Ackerman T. P., McKay C. P., and Turco R. P. 1983. Environmental effects of an impact-generated dust cloud: Implications for the Cretaceous-Tertiary extinctions. *Science* 219:287–289.
- Pope K. O., Baines K. H., Ocampo A. C., and Ivanov B. A. 1994. Impact winter and the Cretaceous/Tertiary extinctions: Results of a Chicxulub asteroid impact model. *Earth and Planetary Science Letters* 128:719–725.
- Pope K. O., Baines K. H., Ocampo A. C., and Ivanov B. A. 1997. Energy, volatile production, and climatic effects of the Chicxulub Cretaceous/Tertiary impact. *Journal of Geophysical Research* 102:21,645–21,664.
- Ramaswamy V. 1992. Explosive start to last ice age. *Nature* 359:14.
- Shoemaker E. M. and Shoemaker C. S. 1996. The Proterozoic impact record of Australia. *Journal of Australian Geology and Geophysics* 16:379–398.
- Shuvalov V. V. 1999. Atmospheric plumes created by meteoroids impacting the Earth. *Journal of Geophysical Research* 104:5877–5890.
- Shuvalov V. V. and Trubetskaya I. A. 2007. Numerical modeling of the formation of the Eltanin submarine impact structure. *Solar System Research* 41:56–64.
- Spray J. G., Kelley S. P., and Dence M. R. 1999. The Strangways impact structure, Northern Territory, Australia: Geological setting and laser probe ⁴⁰Ar/³⁹Ar geochronology. *Earth and Planetary Science Letters* 172:199–211.
- Stern R. J. and Miller N. R. 2018. Did the transition to plate tectonics cause Neoproterozoic Snowball Earth? *Terra Nova* 30:87–94.
- Toon O. B., Zahnle K., Morrison D., Turco R. P., and Covey C. 1997. Environmental perturbations caused by the impacts of asteroids and comets. *Reviews of Geophysics* 35:41–78.
- Umeda Y., Takase A., Fukunaga N., Sekine T., Kobayashi T., Furukawa Y., and Kakegawa T. 2017. Morphological changes of olivine grains reacted with amino acid solutions by impact process. *Physics and Chemistry of Minerals* 44:203–212.
- Werner S. C. and Ivanov B. A. 2015. Exogenic dynamics, cratering, and surface ages (Chapter 10.10). In *Treatise on Geophysics*, 2nd ed, edited by Schubert G. Oxford, UK: Elsevier. pp. 327–365.
- Williams G. E. 2008. Proterozoic (pre-Ediacaran) glaciation and the high obliquity, low-latitude ice, strong seasonality (HOLIST) hypothesis: Principles and tests. *Earth-Science Reviews* 87:61–93.
- Zahnle K. J. 1990. Atmospheric chemistry by large impacts. In *Global catastrophes in Earth history*, edited by Sharpton V. and Ward P. GSA Special Paper 247. Boulder, Colorado: Geological Society of America. pp. 271–288.
- Zumsprekel H. and Bischoff L. 2005. Remote sensing and GIS analyses of the Strangways impact structure, Northern Territory. *Australian Journal of Earth Sciences* 52:621–630.
-